

Supplementary Information

Improving the performance of portable aerosol size spectrometers for building dense monitoring networks

Yiran Li, Jiming Hao and Jingkun Jiang*

State Key Joint Laboratory of Environment Simulation and Pollution Control, School of Environment, Tsinghua University, Beijing, 100084, China

*To whom correspondence should be addressed: jiangjk@tsinghua.edu.cn

1. Measurement of the combined factor of the transfer function, CPC detection efficiency, and penetration efficiency of the modified NanoScan SMPS

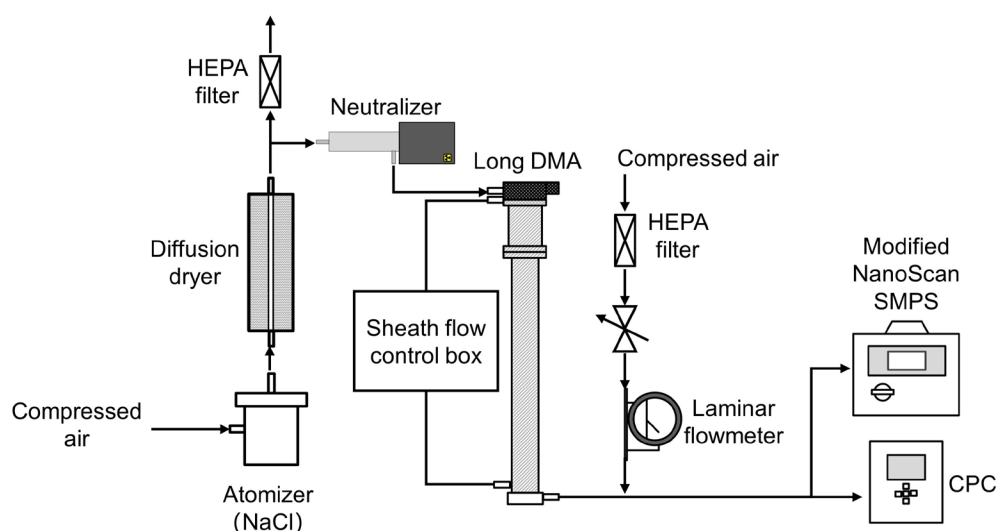


Figure S1. Instrument setup for measuring the combined factor of the transfer function, CPC detection efficiency, and penetration efficiency of the modified NanoScan SMPS

Retrieving the inverted PNSDs measured by the modified NanoScan SMPS requires a data inversion routine similar to those of the SMPS, but the transfer function, CPC detection efficiency, and penetration efficiency need to be measured first. In this study, we used the instrument set-up as shown in Figure S1 to measure the combined factor of them. This is similar to the Tandem DMA method and an iterative deconvolution procedure is used to analyze the data.¹ Polydisperse NaCl aerosols generated by a home-made collision atomizer with a dryer are conditioned by a soft X-ray charger (Model 3087, TSI corp.) and then classified with a long DMA (Model 3081, TSI corp.). The classified monodisperse aerosols are then split and the modified NanoScan SMPS and a CPC (Model 3772, TSI corp.) are measured in parallel. During each measurement period, the voltage of the long DMA was fixed and the voltage of the radial DMA on the modified NanoScan SMPS would scan for 120 seconds. The scan would repeat four times for each selected size. The measured concentrations by CPC are denoted as N_1 and averaged values during each scan were used. The number concentrations from the modified NanoScan SMPS are denoted as N_2 . The ratio between N_1 and N_2 can be expressed by the transfer functions of the long DMA and the radial DMA as follows:²

$$\frac{N_2}{N_1} = \frac{\int_{Z_{p1}^* - \Delta Z_{p1}}^{Z_{p1}^* + \Delta Z_{p1}} \Omega_1(Z_p, Z_{p1}^*) \cdot \Omega_2(Z_p, Z_{p2}^*) \cdot \eta_{\text{CPC}}(Z_{p2}^*) \cdot \eta_{\text{pene}}(Z_{p2}^*) dZ_p}{\int_{Z_{p1}^* - \Delta Z_{p1}}^{Z_{p1}^* + \Delta Z_{p1}} \Omega_1(Z_p, Z_{p1}^*) dZ_p} \quad (\text{S1})$$

29 where $\Omega_1(Z_p, Z_{p1}^*)$ and $\Omega_2(Z_p, Z_{p2}^*)$ are the transfer functions of the long DMA and the radial
 30 DMA, respectively. Z_{p1}^* is the electrical mobility of the particles classified by long DMA and
 31 Z_{p2}^* is the central electrical mobility of the particles measured by radial DMA; ΔZ_{p1} is the half-
 32 width of $\Omega_1(Z_p, Z_{p1}^*)$. $\eta_{\text{CPC}}(Z_{p2}^*)$ is the CPC detection efficiency (on the NanoScan SMPS) for
 33 particles with electrical mobility of Z_{p2}^* , and $\eta_{\text{pene}}(Z_{p2}^*)$ is the penetration efficiency through the
 34 modified NanoScan SMPS for particles with electrical mobility of Z_{p2}^* , both of which are
 35 assumed to be constant between $Z_{p1}^* - \Delta Z_{p1}$ to $Z_{p1}^* + \Delta Z_{p1}$. Here we use triangular-shaped transfer
 36 functions for both DMAs:^{1,3}

$$\Omega_1(Z_p, Z_{p1}^*) = \frac{\alpha_1}{2\beta_1} \left(\left| \frac{Z_{p1}^*}{Z_p} - (1 + \beta_1) \right| + \left| \frac{Z_{p1}^*}{Z_p} - (1 - \beta_1) \right| - 2 \left| \frac{Z_{p1}^*}{Z_p} - 1 \right| \right) \quad (\text{S2})$$

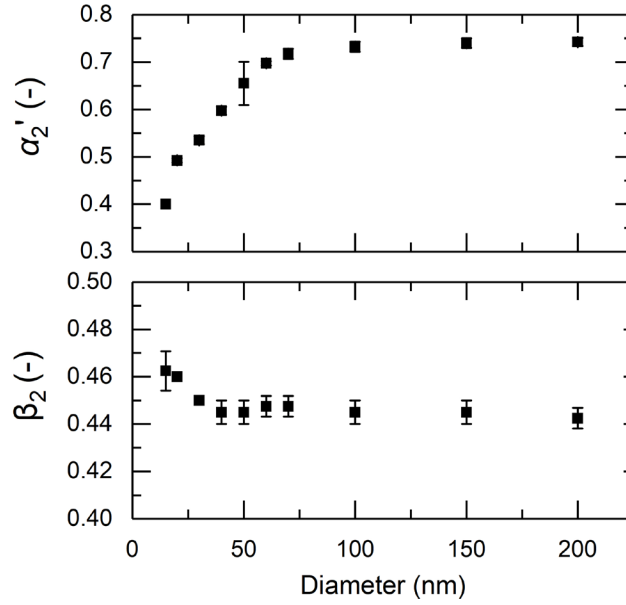
$$\Omega_2(Z_p, Z_{p2}^*) = \frac{\alpha_2}{2\beta_2} \left(\left| \frac{Z_{p2}^*}{Z_p} - (1 + \beta_2) \right| + \left| \frac{Z_{p2}^*}{Z_p} - (1 - \beta_2) \right| - 2 \left| \frac{Z_{p2}^*}{Z_p} - 1 \right| \right) \quad (\text{S3})$$

37 where α_1 and α_2 are the heights of the transfer functions of long DMA and radial DMA, and β_1
 38 and β_2 are the half-widths of the transfer functions of long DMA and radial DMA. A combined
 39 factor of the transfer function, CPC detection efficiency, and penetration efficiency of the
 40 modified NanoScan SMPS are defined as:

$$\Omega_2'(Z_p, Z_{p2}^*) = \frac{\alpha_2'}{2\beta_2} \left(\left| \frac{Z_{p2}^*}{Z_p} - (1 + \beta_2) \right| + \left| \frac{Z_{p2}^*}{Z_p} - (1 - \beta_2) \right| - 2 \left| \frac{Z_{p2}^*}{Z_p} - 1 \right| \right) \quad (\text{S4})$$

$$\alpha_2' = \eta_{\text{CPC}}(Z_{p2}^*) \cdot \eta_{\text{pene}}(Z_{p2}^*) \quad (\text{S5})$$

41 With the known α_1 and β_1 , a deconvolution procedure based on the method of least squares
 42 is used to retrieve α_2' and β_2 .¹ Besides, using two identical long DMAs one can retrieve the
 43 values of α_1 and β_1 , which are determined in this study to be 0.91 and 0.11, respectively. The
 44 results of $\Omega_2'(Z_p, Z_{p2}^*)$ are shown in Fig. S2, which is incorporated in the data inversion routine
 45 described below.



46

47 **Figure S2.** Results of the combined factor of the transfer function, CPC detection efficiency, and
 48 penetration efficiency of the modified NanoScan SMPS

49 **2. Calculation of ion mobility ratio and PNSDs for the bipolar data**

50 With the bipolar data from the reference SMPS and the modified NanoScan SMPS, the ion
 51 mobility ratio can be calculated with a formula:⁴

$$x = \exp[\ln(R_{d_p}^+ / R_{d_p}^-) / 2] \quad (S6)$$

52 where $R_{d_p}^+$ and $R_{d_p}^-$ are the raw concentrations of positively and negatively charged particles in
 53 the size of d_p (cm^{-3}). d_p is a size with little influence from larger aerosols carrying multiple
 54 charges and can be found with an empirical method.⁴

55 With the ion mobility ratios, charge fractions can be calculated:⁴

$$f(\pm q, d_p) = \frac{e}{\sqrt{4\pi^2 \epsilon_0 \alpha d_p k_B T}} \exp \frac{-[\pm q - \frac{2\pi\epsilon_0 \alpha d_p k_B T}{e^2} \ln(x)]^2}{2 \frac{2\pi\epsilon_0 \alpha d_p k_B T}{e^2}} \quad (S7)$$

$$\alpha = \begin{cases} 0.9630 \times \exp\left(\frac{7.6019}{d_p + 2.2476}\right) & q = 1 \\ 0.9826 + 0.9435 \exp(-0.0478 d_p) & q = 2 \\ 1 & q \geq 3 \end{cases}$$

56 where $f(\pm q, d_p)$ is the fraction of size d_p particles carrying $\pm q$ elementary charges
 57 (dimensionless); e is the elementary charge (C); ϵ_0 is the permittivity of vacuum ($\text{C}^2 \cdot \text{N}^{-1} \cdot \text{m}^{-2}$); k_B
 58 is the Boltzmann's constant ($\text{J} \cdot \text{K}^{-1}$); T is the temperature (K); α is the correction coefficient
 59 (dimensionless).

60 The relationship between measured raw concentrations and the desired concentration of
 61 aerosols that are being measured is:

$$R_{d_p} = \int_0^{\infty} N(d_p) \cdot G(i, d_p) \cdot dd_p, \quad i = 1, 2, \dots, 30 \quad (\text{S8})$$

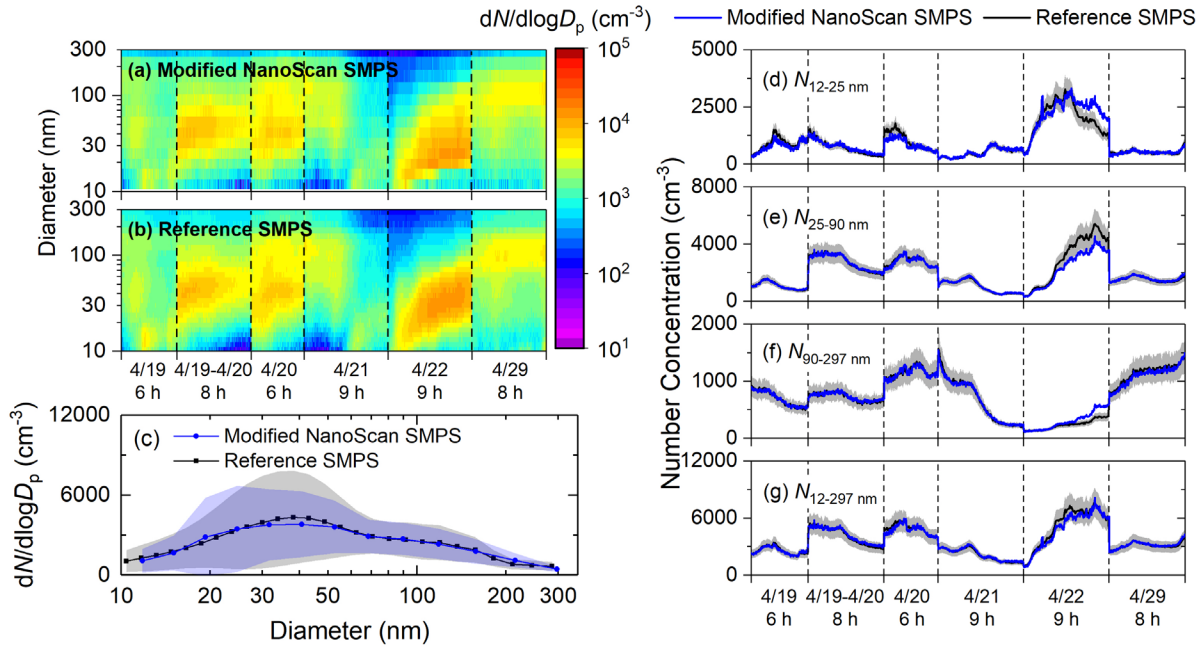
$$G(i, d_p) = Q_a \sum_{q=1}^{\infty} [f(+q, d_p) + f(-q, d_p)] \cdot P(q, i, d_p) \cdot dd_p \quad (\text{S9})$$

62 Where R_{d_p} is the sum of $R_{d_p}^+$ and $R_{d_p}^-$ (cm^{-3}), $N(d_p)dd_p$ is the number concentration of all
 63 particles of size d_p (cm^{-3}), Q_a is the sample flowrate ($\text{cm}^3 \cdot \text{s}^{-1}$), $P(q, i, d_p)$ is a combined factor
 64 of the transfer function of the DMA, counting efficiency of the CPC and penetration efficiency
 65 through the SMPS systems. For the reference SMPS, the transfer function of the long DMA was
 66 calculated by formula from Knutson and Whitby (1975)⁵, the counting efficiency of the CPC was
 67 calculated with parameters provided by the instrument manual, and penetration efficiency was
 68 calculated with the equivalent pipe length method.⁶ For the modified NanoScan SMPS,
 69 $P(q, i, d_p)$ was obtained with the method described above. A linear inversion algorithm was used
 70 to obtain $N(d_p)dd_p$ from R_{d_p} .⁷

71 3. Calculation of parameters that characterize the PNSDs

72 For number concentrations in nucleation mode, Aitken mode, accumulation mode, and the
 73 whole measured size range, the specific size range for each mode is not unified but set to be
 74 different for the original NanoScan SMPS and the modified NanoScan SMPS. The reason is that
 75 using a unified size range for two instruments requires interpolation of PNSDs to the same size
 76 bins, while the original NanoScan SMPS and the modified NanoScan SMPS have different
 77 midpoints of size bins and the bins are wide, meaning that interpolation would cause extra
 78 uncertainty. Besides, PNSDs measured by the original NanoScan SMPS and the modified
 79 NanoScan SMPS are not directly compared to each other, but both with those measured by the
 80 reference SMPS. Consistency with the reference SMPS is then compared to illustrate their
 81 performance. For the original NanoScan SMPS, these size ranges are 12 - 27nm (nucleation
 82 mode), 27 - 87 nm (Aitken mode), 87 - 274 nm (accumulation mode), and 12 - 274 nm (the
 83 whole size range). For the modified NanoScan SMPS, these size ranges are 12 - 25nm
 84 (nucleation mode), 25 - 90 nm (Aitken mode), 90 - 297 nm (accumulation mode), and 12 - 297
 85 nm (the whole size range). The PNSDs obtained by the reference SMPS are linearly interpolated
 86 to the size bin of either the original NanoScan SMPS or the modified NanoScan SMPS,
 87 depending on which one it was being compared to, and number concentrations in different
 88 modes are then integrated. The geometric mean diameter and geometric standard deviations are
 89 calculated based on the PNSDs without interpolation for the reference SMPS.

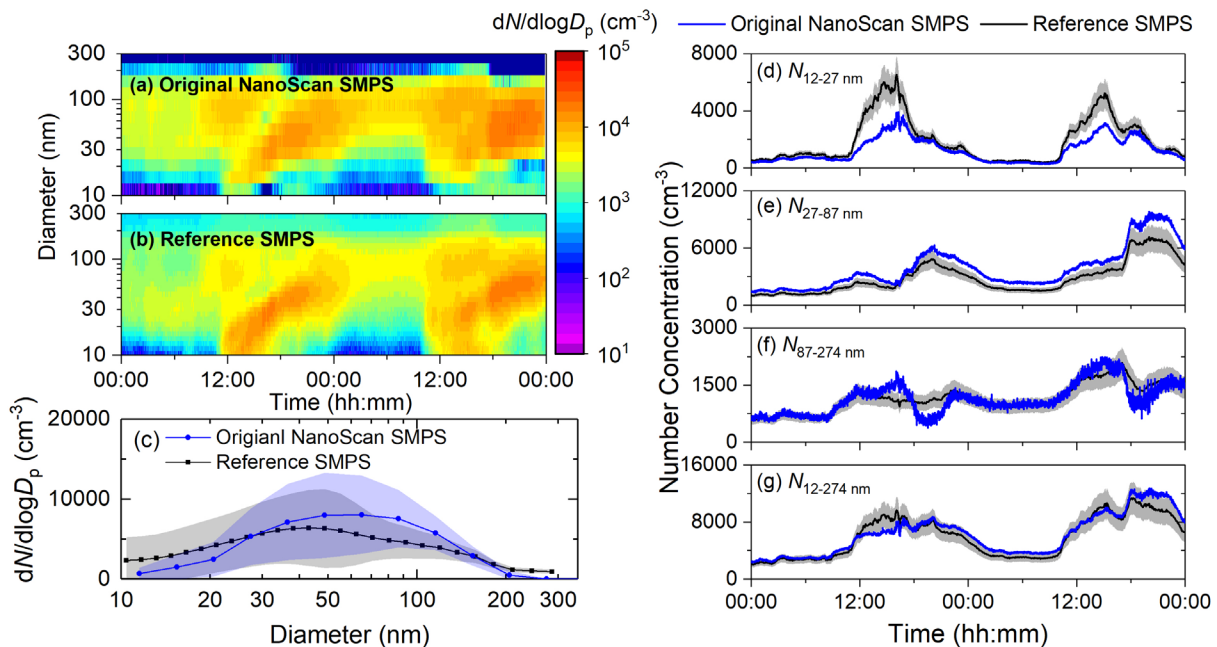
90 4. Indoor aerosols measured by the modified NanoScan SMPS and the reference SMPS



91

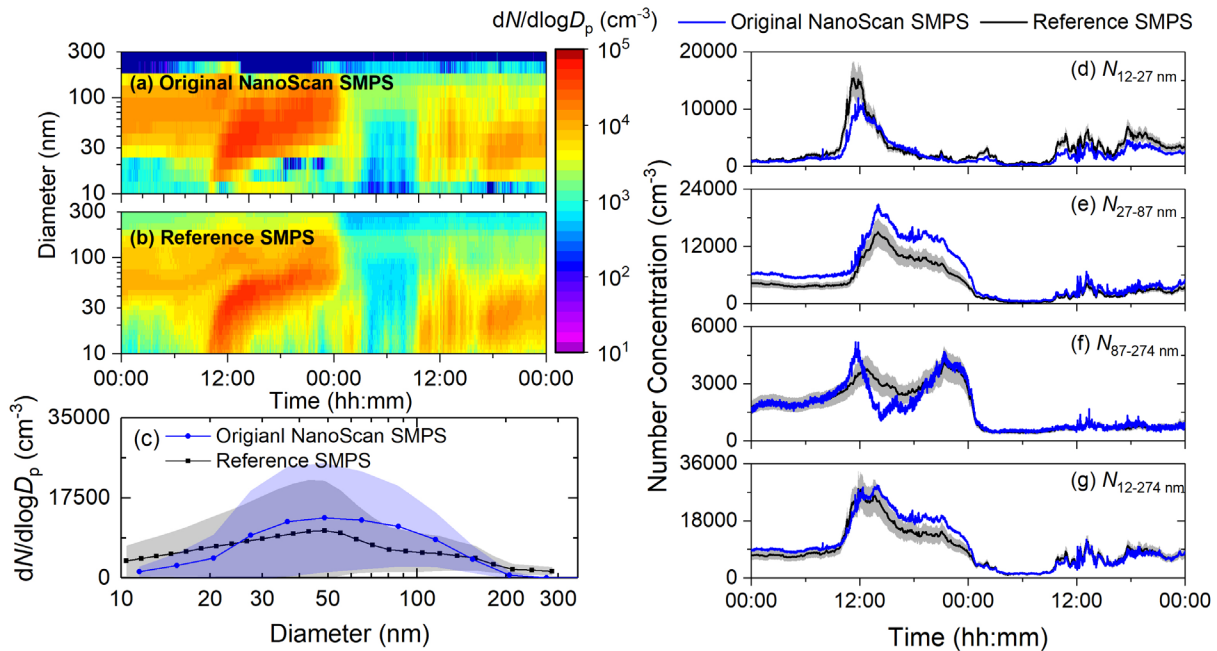
92 **Figure S3.** PNSDs of indoor aerosols for a total of 46 hours by (a) the modified NanoScan
 93 SMPS and (b) the reference SMPS. (c) The averaged size distributions and standard deviations
 94 during the measurement period, as denoted by line and shaded area, respectively. Integrated
 95 number concentrations in the size range of (d) 12 - 25 nm, (e) 25 - 90 nm, (f) 90 - 297 nm, (g) 12
 96 - 297 nm of measured size distributions are shown, and the shaded area represent $\pm 20\%$ range of
 97 the reference SMPS. The time resolution for the PNSDs and thus the calculated parameters
 98 measured by the modified NanoScan SMPS and the reference SMPS are 75 s and 5 min,
 99 respectively.

100 **5. Time series of indoor and outdoor aerosols for the original NanoScan SMPS**



101

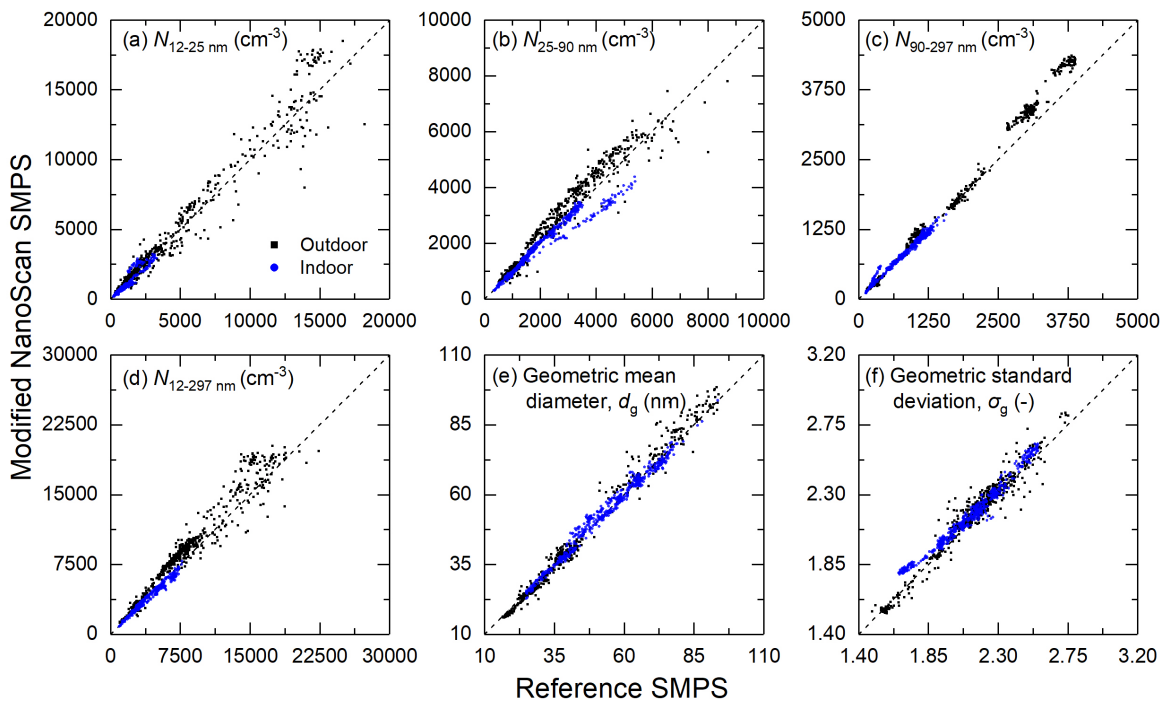
102 **Figure S4.** PNSDs of indoor aerosols for a total of 48 hours by (a) the original NanoScan SMPS
 103 and (b) the reference SMPS. (c) The averaged size distributions and standard deviations during
 104 the measurement period, as denoted by line and shaded area, respectively. Integrated number
 105 concentrations in the size range of (d) 12 - 27nm, (e) 27 - 87 nm, (f) 87 - 274 nm, (g) 12 - 274
 106 nm of measured size distributions are shown, and the shaded area represent $\pm 20\%$ range of the
 107 reference SMPS. The time resolution for the PNSDs and thus the calculated parameters
 108 measured by the original NanoScan SMPS and the reference SMPS are 1 min and 5 min,
 109 respectively.



110

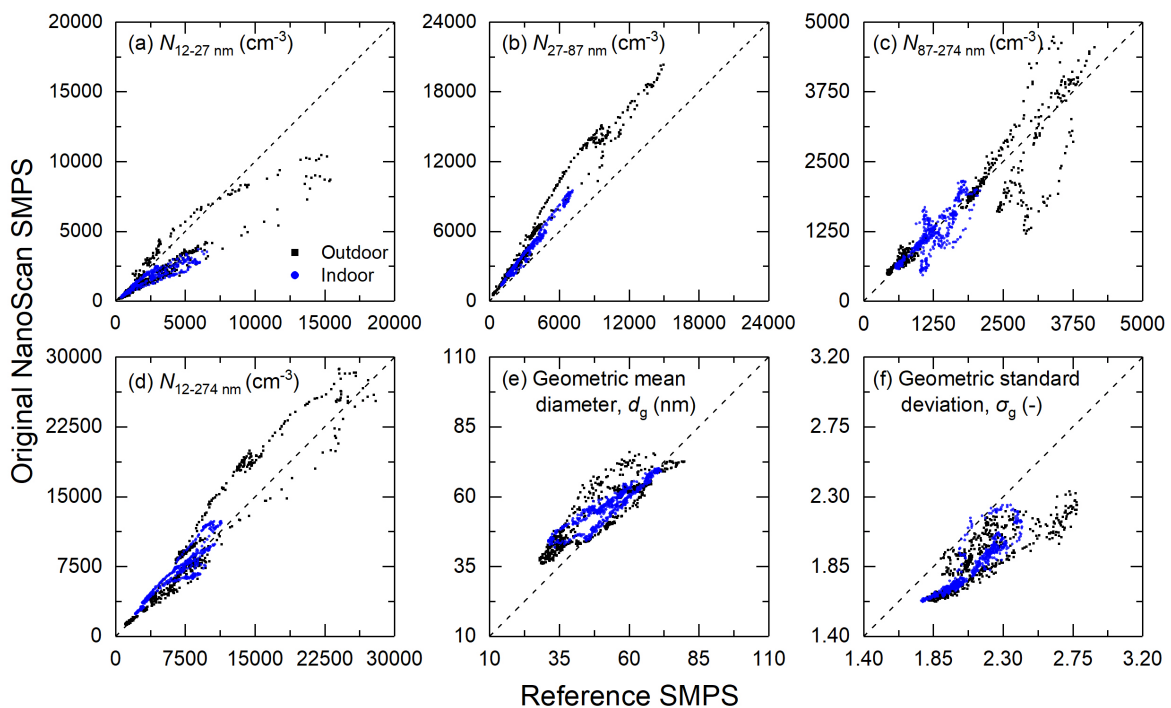
111 **Figure S5.** PNSDs of outdoor aerosols for a total of 48 hours by (a) the original NanoScan
 112 SMPS and (b) the reference SMPS. (c) The averaged size distributions and standard deviations
 113 during the measurement period, as denoted by line and shaded area, respectively. Integrated
 114 number concentrations in the size range of (d) 12 - 27nm, (e) 27 - 87 nm, (f) 87 - 274 nm, (g) 12
 115 - 274 nm of measured size distributions are shown, and the shaded area represent $\pm 20\%$ range of
 116 the reference SMPS. The time resolution for the PNSDs and thus the calculated parameters
 117 measured by the original NanoScan SMPS and the reference SMPS are 1 min and 5 min,
 118 respectively.

119 **6. Scatter plots for all measuring periods using indoor and outdoor aerosols**



120

121 **Figure S6.** Comparing size distributions of outdoor and indoor aerosols for all measurement
 122 periods by the reference SMPS (x-axis) and the modified NanoScan SMPS (y-axis). Integrated
 123 number concentrations in the size range of (a) 12 - 25 nm, (b) 25 - 90 nm, (c) 90 - 297 nm, (d) 12
 124 - 297 nm as well as (e) geometric mean diameter and (f) geometric standard deviation of
 125 measured size distributions are shown. The time resolution for the data is 5 min. Data points are
 126 shown in circles (blue) for indoor aerosols, and in squares (black) for outdoor aerosols. The dash
 127 lines are for guiding the eyes.



128

129 **Figure S7.** Comparing size distributions of outdoor and indoor aerosols for all measurement
130 periods by the reference SMPS (x-axis) and the original NanoScan SMPS (y-axis). Integrated
131 number concentrations in the size range of (a) 12 - 27nm, (b) 27 - 87 nm, (c) 87 - 274 nm, (d) 12
132 - 274 nm as well as (e) geometric mean diameter and (f) geometric standard deviation of
133 measured size distributions are shown. The time resolution for the data is 5 min. Data points are
134 shown in circles (blue) for indoor aerosols, and in squares (black) for outdoor aerosols. The dash
135 lines are for guiding the eyes.

136

137 Reference

- 138 1. F. Stratmann, T. Kauffeldt, D. Hummes and H. Fissan, Differential Electrical Mobility
139 Analysis: A Theoretical Study, *Aerosol Sci Tech*, 1997, **26**, 368-383.
- 140 2. W. L. Li, L. Li and D. R. Chen, Technical note: A new deconvolution scheme for the
141 retrieval of true DMA transfer function from tandem DMA data, *Aerosol Sci Tech*, 2006,
142 **40**, 1052-1057.
- 143 3. S. H. Zhang, Y. Akutsu, L. M. Russell, R. C. Flagan and J. H. Seinfeld, Radial
144 Differential Mobility Analyzer, *Aerosol Sci Tech*, 1995, **23**, 357-372.
- 145 4. X. T. Chen and J. Jiang, Retrieving the ion mobility ratio and aerosol charge fractions for
146 a neutralizer in real-world applications, *Aerosol Sci Tech*, 2018, **52**, 1145-1155.
- 147 5. E. O. Knutson and K. T. Whitby, Aerosol classification by electric mobility: apparatus,
148 theory, and applications, *J Aerosol Sci*, 1975, **6**, 443-451.
- 149 6. A. Wiedensohler, W. Birmili, A. Nowak, A. Sonntag, K. Weinhold, M. Merkel, B.
150 Wehner, T. Tuch, S. Pfeifer, M. Fiebig, A. M. Fjaraa, E. Asmi, K. Sellegri, R. Depuy, H.
151 Venzac, P. Villani, P. Laj, P. Aalto, J. A. Ogren, E. Swietlicki, P. Williams, P. Roldin, P.
152 Quincey, C. Hüglin, R. Fierz-Schmidhauser, M. Gysel, E. Weingartner, F. Riccobono, S.
153 Santos, C. Gruning, K. Faloon, D. Beddows, R. M. Harrison, C. Monahan, S. G. Jennings,
154 C. D. O'Dowd, A. Marinoni, H. G. Horn, L. Keck, J. Jiang, J. Scheckman, P. H.
155 McMurry, Z. Deng, C. S. Zhao, M. Moerman, B. Henzing, G. de Leeuw, G. Loschau and
156 S. Bastian, Mobility particle size spectrometers: harmonization of technical standards and
157 data structure to facilitate high quality long-term observations of atmospheric particle
158 number size distributions, *Atmos Meas Tech*, 2012, **5**, 657-685.
- 159 7. D. E. Hagen and D. J. Alofs, Linear Inversion Method to Obtain Aerosol Size
160 Distributions from Measurements with a Differential Mobility Analyzer, *Aerosol Sci
161 Tech*, 1983, **2**, 465-475.
- 162 8. X. T. Chen, P. H. McMurry and J. Jiang, Stationary characteristics in bipolar diffusion
163 charging of aerosols: Improving the performance of electrical mobility size spectrometers,
164 *Aerosol Sci Tech*, 2018, **52**, 809-813.

165